ChemComm

COMMUNICATION

View Article Online
View Journal | View Issue

Cite this: *Chem. Commun.*, 2019, **55**, 3065

Received 20th December 2018,
Accepted 8th February 2019

DOI: 10.1039/c8cc10074h

rsc.li/chemcomm

Hybridization chain reaction-based nanoprobe for cancer cell recognition and amplified photodynamic therapy†

Mengyi Xiong,[a] Qiming Rong,[a] Gezhi Kong,[a] Chan Yang,[a] Yan Zhao,[ab] Feng-Li Qu,*[b] Xiao-Bing Zhang *[a] and Weihong Tan [a]

Precision diagnosis and effective treatment are the cores of early cancer therapy. Here, for the first time, we report a hybridization chain reaction-based nanoprobe for selective and sensitive cancer cell recognition and amplified photodynamic therapy.

Cancer has always been one of the highest mortality diseases for human life. Millions of patients die from cancer each year due to the rapid proliferation and widespread metastasis of cancer cells.[1–3] Despite the tremendous advances in diagnostic technologies, such as ultrasound (US) imaging, computer tomography (CT) imaging and magnetic resonance imaging (MRI),[4] a substantial number of cancer patients are still diagnosed with metastasis. This is because conventional medical imaging techniques cannot be applied to sensitively and accurately detect epithelial tissues, where more than 80% of early cancers take place.[5] Therefore, precision diagnoses and effective treatments are urgently needed to prevent and cure cancer. In recent years, DNA oligonucleotide fluorescent biosensors, with which multiple cancer biomarkers such as small molecules, mRNA, proteins, cancer cells and even tumor tissues can be tracked in a minimally invasive way, have shown their potential to offer excellent solutions to this issue.[6–8] Moreover, programmable DNA sensors can be improved with various amplification strategies for ultrasensitive detection, including rolling circle amplification (RCA),[9] catalytic hairpin assembly (CHA)[10] and the hybridization chain reaction (HCR).[11] Among these amplification strategies, HCR has been widely used for RNA detection and imaging in living cells and is therefore able to distinguish cancer cells from normal cells through a specific RNA target.[12] In addition, the long double-strand DNA generated by HCR is also a desirable drug carrier for cancer therapy.[13] Consequently, HCR based DNA sensors or nanodevices possess great potential as favorable methods for precise cancer diagnosis and therapy.[14]

In the battle with cancer, all sorts of therapeutic strategies, such as chemotherapy, radiation therapy and surgery, are generally introduced in clinical cancer therapy. The common defects of these strategies include low selectivity, drug resistance and systemic toxicity, each of which can result in an unsatisfactory efficacy.[15] With the persistent seeking and development of innovative cancer treatment, photodynamic therapy (PDT) was developed to reduce the side-effects in cancer therapy. PDT takes advantage of a non-toxic and tumor-localizing photosensitizer, which can be activated by focused light to produce cytotoxic reactive singlet oxygen ($^1O_2$) to cause the cell death.[16] Though $^1O_2$ has a limited lifespan and diffusion distance that exhibit relatively low systemic toxicity, efficient and reliable PDT still demands a good selectivity toward the targeted cells. Otherwise, the surrounding normal tissues are still at risk of being damaged. Therefore, the accurate activation of photosensitizer at the tumor site to kill cancer cells selectively remains a challenge for PDT.

To improve the selectivity and reduce the side effects of PDT activatable systems are introduced to control the specificity of the photosensitizer.[17–20] Here, we, for the first time, construct an intracellular HCR amplification nanoprobe to selectively recognize cancer cells in combination with PDT for therapy. As displayed in Scheme 1, chlorin e6 (Ce6) is a typical photosensitizer which can efficiently produce $^1O_2$ under the irradiation of light and the GO nanosheet can be used as both the cellular transporter and fluorescence quencher, which can keep the photosensitizer nontoxic. In this proposal, the Ce6 was conjugated to the 5′-terminal of two DNA hairpin structures (rH_1 and H_2), then the hairpin structures were adsorbed on the GO nanosheet to inactivate the Ce6. In addition, the HCR was designed to be triggered by the mRNA of human mutT homologue (mMTH1), which is usually regarded as a biomarker of cancer cells.[21,22] Once this nanoprobe is delivered into the cytoplasm of cancer cells the mMTH1 will trigger the HCR to

[a] *Molecular Science and Biomedicine Laboratory, State Key Laboratory of Chemo/Biosensing and Chemometrics, College of Chemistry and Chemical Engineering, Hunan University, Changsha 410082, P. R. China. E-mail: xbzhang@hnu.edu.cn*

[b] *The Key Laboratory of Life-Organic Analysis, College of Chemistry and Chemical Engineering, Qufu Normal University, Qufu 273165, P. R. China. E-mail: qflhn@126.com*

† Electronic supplementary information (ESI) available: Experimental details, one table and five figures. See DOI: 10.1039/c8cc10074h

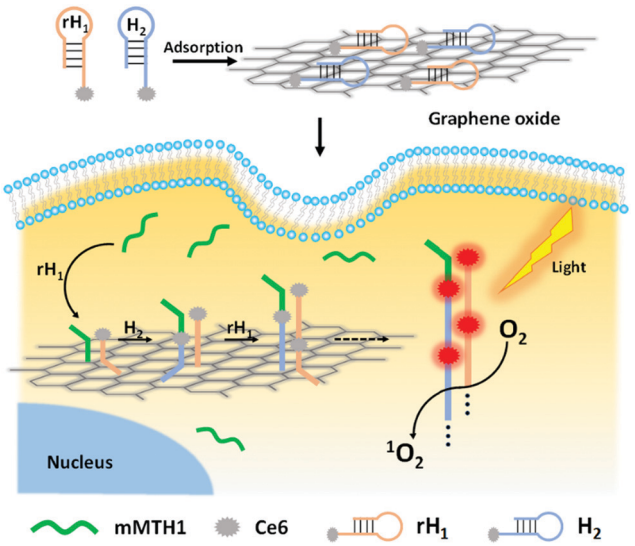

Scheme 1 Selective recognition of cancer cells and amplified photodynamic therapy based on the HCR and GO nanosheets.

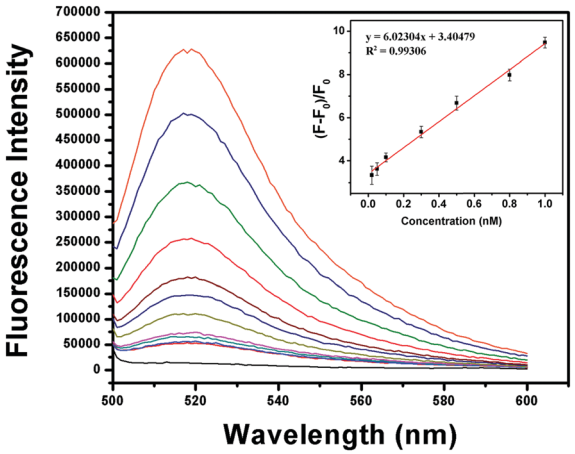

Fig. 1 Fluorescence spectra of the mixture solutions with 25 μg mL^{-1} nano-compound and various concentrations of mMTH1 target. Inset: Calibration curve of fluorescence enhancement corresponding target concentrations (0.02, 0.05, 0.1, 0.3, 0.5, 0.8 and 1.0 nM). The error bars represent the SD calculated from three independent experiments. Excitation wavelength = 494 nm, slit width = 2 nM.

form long dsDNA. Then, the dsDNA can be released from the GO nanosheet, due to the weak affinity between the GO nanosheet and dsDNA, which means abundant Ce6 can be activated to produce $^1O_2$ for amplified PDT. In contrast, when the nanoprobe is delivered into normal cells, the Ce6 cannot be activated since the target mMTH1 is barely present. In this way, the cancer cells are selectively distinguished and the PDT efficiency will be largely amplified, even in a low level of target mMTH1.

Initially, fluorescein (FAM) labeled hairpin structures (rH_1 and H_2) was utilized to verify our hypothesis and to optimize the strategy (sequences are displayed in Table S1, ESI†). Gel electrophoresis analysis was used to demonstrate the existence of long dsDNA generated by this well-designed HCR. As shown in Fig. S1 (ESI†), the long dsDNA was observed when the target strand was added, which indicated the feasible occurrence of HCR in the presence of mMTH1. Interestingly, the length of the dsDNA decreased with increasing concentrations of the target, because the consumption of hairpins was determined by the initial molar ratio of the trigger to hairpin structures.[13] Then, the GO nanosheets were generated through ultrasound and atomic force microscope (AFM) imaging indicated the height of the nanosheets was ~1.5 nm (Fig. S2, ESI†). The quenching ability of the GO nanosheet was evaluated using the fluorescence intensity of the FAM-labeled hairpins with different concentrations of the GO nanosheet. As displayed in Fig. S2 (ESI†), the addition of 40 μg mL^{-1} GO nanosheet could efficiently quench the fluorescence of 10 nM rH_1 and H_2, which indicated the outstanding quenching capability of the GO nanosheet. To improve the sensitivity of this nanoprobe, we further optimized the amounts of hairpin structures and GO nanosheets. Various concentrations of rH_1/H_2 were mixed with 500 μg mL^{-1} GO nanosheet, then 50 nM target was used to trigger the HCR. The signal-to-background ratio was employed to evaluate the sensitivity of the nanoprobe. As shown in Fig. S3 (ESI†), with increasing concentrations of rH_1/H_2 from 10 nM to 5 μM, the signal-to-background ratio rose at first and then decreased. This is because, with a low rH_1/H_2 concentration, the hairpin structures can hardly be released from the GO nanosheet due to the strong interaction between them, which reduces the sensitivity of the nanoprobe. However, when the concentration of rH_1/H_2 increased excessively, the fluorescence of FAM on the hairpin structures could not be quenched efficiently, which induced a high background signal. The optimal concentration of rH_1/H_2 to achieve a highly sensitive nanoprobe was demonstrated to be 500 nM. Therefore, a stock solution consisting of 500 μg mL^{-1} GO and 0.5 μM rH_1/H_2 was prepared for further use, and the concentration of this mixture was represented by the concentration of GO. Under the optimized conditions, the sensitivity of this nanoprobe with various concentrations of the target was also investigated. As shown in Fig. 1, a dramatic increase in the fluorescence intensity was observed with increasing concentration of target. The insert indicates an excellent linear relationship when the concentration of target ranged from 0 to 1 nM, with a detection limit of 6.87 pM (3 s per slope), which suggested this nanoprobe was a sensitive strategy for cancer diagnosis (a plot of ratios for fluorescence enhancement is displayed in Fig. S4, ESI†).

Though the GO nanosheet based HCR has been reported to image endogenous RNA in living cells,[23] in order to investigate the diagnostic ability and the location of this HCR/GO nanoprobe in living cells, live-cell confocal laser scanning microscopy (CLSM) was used to image the mMTH1 in cells. The excitation wavelengths of Cy3 and LysoTracker Green were used in this experiment. The results are shown in Fig. 2A, there is an obvious fluorescence signal in HeLa cells, while almost no fluorescence signal in normal cells is observed. The co-localization of sensor and lysosomes implied that the nanoprobe was partly trapped in lysosomes. Additionally, flow cytometry was used to investigate the ability of this strategy to distinguish cancer cells from normal cells. As expected, the HeLa cells exhibited a stronger fluorescence

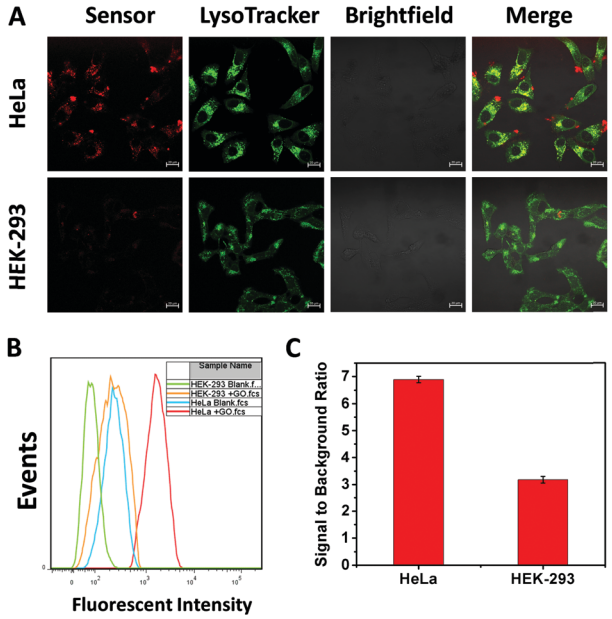

Fig. 2 (A) Confocal images of HEK-293 and HeLa cells. The Cy3 and LysoTracker Green were used as the excitation channels (Ex = 543 nm and 488 nm), scale bar = 20 μm. (B) Flow cytometry assay of mMTH1 triggered HCR in HeLa and HEK-293 cells. (C) The fluorescence signal to background ratio calculated by flow cytometry.

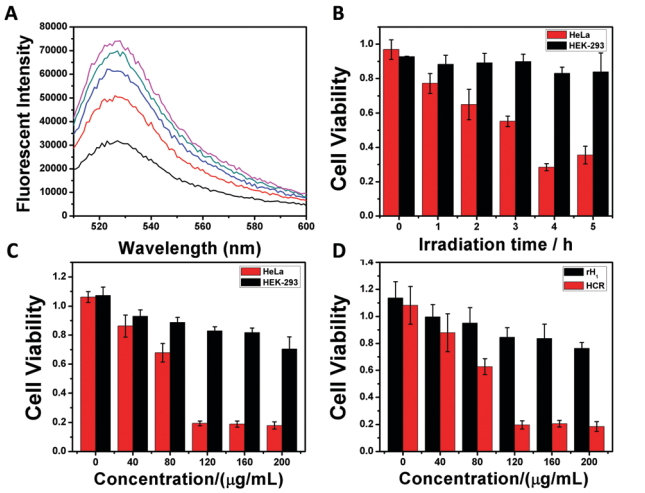

Fig. 3 (A) The fluorescence signal of singlet oxygen sensor green (SOSG) for $^1O_2$ monitoring. (B) The cell viability of HeLa cells and HEK-293 cells under 120 μg mL^{-1} Ce6-HCR/GO mixture after different irradiation times. (C) The cell viability of HeLa cells and HEK-293 cells with different concentrations of Ce6-HCR/GO mixture. (D) The cell viability of HeLa cells *versus* different concentrations of Ce6-rH$_1$/GO or Ce6-HCR/GO mixture.

signal than the HEK-293 cells when the nanoprobe was applied (Fig. 2B and Fig. S5, ESI†). The higher signal to background ratio from the HeLa cells indicated that the HCR/GO nanoprobe could be used to distinguish cancer cells from normal cells (Fig. 2C).

After verifying the feasibility of this nanoprobe for cancer cell recognition, we further tested the PDT efficacy. The Ce6 modified hairpin structures (Ce6-rH$_1$ and Ce6-H$_2$) were fabricated and identified by high-performance liquid chromatography (HPLC) (the method is described in ESI†). Then, these hairpin structures were adsorbed on the GO nanosheet. To evaluate the productivity of $^1O_2$ in the presence of the target by this nanoprobe, singlet oxygen sensor green (SOSG) was utilized as a detector of $^1O_2$. The reaction between $^1O_2$ and SOSG results in fluorescence enhancement, therefore it can monitor the generation of $^1O_2$ in our nanoprobe. Different concentrations of the target were added to the solution which contained the nano-compound and SOSG, then the solution was irradiated under LED light for 4 hours. As can be seen in Fig. 3A, the fluorescence intensity of SOSG enhanced along with the increase of target concentration, which indicated the mMTH1-dependent generation of $^1O_2$ in this nanoprobe.

To apply this mMTH1-triggered HCR/GO nanoprobe for precise PDT therapy, the HeLa and HEK-293 cell lines were chosen as the target and control respectively. Cell viability was determined using a Cell Titer 96 Cell Proliferation Assay. The absorbance (490 nm) of MTS was recorded and the cell viability was calculated. As displayed in Fig. 3B, evident toxicity to HeLa cells was observed with the increase of irradiation time, and the result implied the cancer cells were sufficiently killed by 4 hours of irradiation under LED light, while the normal cells were well protected. The dosage for therapy was also investigated, a dramatic difference in cytotoxicity toward cancer and normal cells was found with the increasing concentration of this nanoprobe (Fig. 3C). However, the viability of normal cells was slightly reduced under a high dose of the nanoprobe, which might be caused by circuit leakage of the DNA sensor.[24] According to the quantitative cell toxicity tests demonstrated above, our Ce6-HCR/GO nanoprobe can kill cancer cells selectively with minimal harm to normal cells.

In addition to the selectivity, the efficiency also plays a vital role in precision cancer therapy. Therefore, the recognition of the trace target which triggered this amplified therapy in our nanoprobe was also investigated. A complementary DNA (rH$_1$) which could hybridize with mMTH1 was used to construct the Ce6-rH$_1$/GO as a negative control. According to the cell viability test in Fig. 3D, in the same level of target, the Ce6-HCR/GO nanoprobe possessed prominent superiority compared with the Ce6-rH$_1$/GO nanoprobe. That is because the HCR/GO nanoprobe activated much more photosensitizer through a catalytic reaction between rH$_1$ and H$_2$ than the non-amplified Ce6-rH$_1$/GO nanosystem. Hence, this activatable PDT could perform efficiently even in low concentrations of trigger.

In conclusion, we successfully developed a HCR-based nanoprobe for accurate cancer PDT for the first time. This nanoprobe employed DNA HCR for cancer cell recognition and amplified PDT therapy, which exhibits excellent selectivity and high PDT efficiency. We believe this universal strategy will expand the application of DNA amplification strategies for precise cancer therapy. By combining the programmable DNA reactions with therapy approaches, more effective treatments may be carried out.

This work was supported by the National Natural Science Foundation of China (21890744) and the Science and Technology Project of Hunan Province (2016RS2009 and 2016WK2002).

Conflicts of interest

The authors declare no competing financial interests.

Notes and references

1 S. A. Belinsky, K. J. Nikula, W. A. Palmisano, R. Michels, G. Saccomanno, E. Gabrielson, S. B. Baylin and J. G. Herman, *Proc. Natl. Acad. Sci. U. S. A.*, 1998, **95**, 11891.
2 S. S. Gambhir, *Nat. Rev. Cancer*, 2002, **2**, 683.
3 S. Nagrath, L. V. Sequist, S. Maheswaran, D. W. Bell, D. Irimia, L. Ulkus, M. R. Smith, E. L. Kwak, S. Digumarthy, A. Muzikansky, P. Ryan, U. J. Balis, R. G. Tompkins, D. A. Haber and M. Toner, *Nature*, 2007, **450**, 1235.
4 W. Wang, J. Zhao, M. Short and H. Zeng, *J. Biophotonics*, 2015, **8**, 527.
5 A. Nijssen, S. Koljenovic, T. C. Bakker Schut, P. J. Caspers and G. J. Puppels, *J. Biophotonics*, 2009, **2**, 29.
6 M. Xiong, H. Zhu, Q. Rong, C. Yang, L. Qiu, X. B. Zhang and W. Tan, *Chem. Commun.*, 2016, **52**, 4679.
7 H. Kuai, Z. Zhao, L. Mo, H. Liu, X. Hu, T. Fu, X. Zhang and W. Tan, *J. Am. Chem. Soc.*, 2017, **139**, 9128.
8 K. Quan, J. Li, J. Wang, N. Xie, Q. Wei, J. Tang, X. Yang, K. Wang and J. Huang, *Chem. Sci.*, 2019, **10**, 1442.
9 M. M. Ali, F. Li, Z. Zhang, K. Zhang, D. K. Kang, J. A. Ankrum, X. C. Le and W. Zhao, *Chem. Soc. Rev.*, 2014, **43**, 3324.
10 C. H. Zhang, Y. Tang, Y. Y. Sheng, H. Wang, Z. Wu and J. H. Jiang, *Chem. Commun.*, 2016, **52**, 13584.
11 S. Bi, S. Yue and S. Zhang, *Chem. Soc. Rev.*, 2017, **46**, 4281.
12 Z. Wu, G. Q. Liu, X. L. Yang and J. H. Jiang, *J. Am. Chem. Soc.*, 2015, **137**, 6829.
13 G. Zhu, J. Zheng, E. Song, M. Donovan, K. Zhang, C. Liu and W. Tan, *Proc. Natl. Acad. Sci. U. S. A.*, 2013, **110**, 7998.
14 K. Ren, Y. Zhang, X. Zhang, Y. Liu, M. Yang and H. Ju, *ACS Nano*, 2018, **12**, 10797.
15 Y. Zhou, X. Liang and Z. Dai, *Nanoscale*, 2016, **8**, 12394.
16 Y. Shen, A. J. Shuhendler, D. Ye, J. J. Xu and H. Y. Chen, *Chem. Soc. Rev.*, 2016, **45**, 6725.
17 J. Wang, G. Z. Zhu, M. X. You, E. Q. Song, M. I. Shukoor, K. J. Zhang, M. B. Altman, Y. Chen, Z. Zhu, C. Z. Huang and W. H. Tan, *ACS Nano*, 2012, **6**, 5070.
18 G. Zheng, J. Chen, K. Stefflova, M. Jarvi, H. Li and B. C. Wilson, *Proc. Natl. Acad. Sci. U. S. A.*, 2007, **104**, 8989.
19 J. Chen, J. F. Lovell, P. C. Lo, K. Stefflova, M. Niedre, B. C. Wilson and G. Zheng, *Photochem. Photobiol. Sci.*, 2008, **7**, 775.
20 D. Han, G. Z. Zhu, C. C. Wu, Z. Zhu, T. Chen, X. B. Zhang and W. H. Tan, *ACS Nano*, 2013, **7**, 2312.
21 X. Li, L. Li, Y. Huang, B. Liu, H. Chi, L. Shi, W. Zhang, G. Li, Y. Niu and X. Zhu, *Biomater. Sci.*, 2017, **5**, 2068.
22 H. Fan, L. Zhang, X. Hu, Z. Zhao, H. Bai, X. Fu, G. Yan, L. H. Liang, X. B. Zhang and W. Tan, *Chem. Commun.*, 2018, **54**, 4310.
23 L. Li, J. Feng, H. Liu, Q. Li, L. Tong and B. Tang, *Chem. Sci.*, 2016, **7**, 1940.
24 X. Sun, B. Wei, Y. Guo, S. Xiao, X. Li, D. Yao, X. Yin, S. Liu and H. Liang, *J. Am. Chem. Soc.*, 2018, **140**, 9979.

